Computer Methods and Programs in Biomedicine 246 (2024) 108056

Contents lists available at ScienceDirect

Computer Methods and Programs in Biomedicine

journal homepage: www.elsevier.com/locate/cmpb

Fluid-structure interaction analysis of the thromboembolic risk in the left atrial appendage under atrial fibrillation: Effect of hemodynamics and morphological features

Giulio Musotto [a,1], Alessandra Monteleone [a,1], Danila Vella [a], Bernardo Zuccarello [b], Ruggero Cannova [b], Andrew Cook [c], Giorgia Maria Bosi [d], Gaetano Burriesci [a,d,*]

[a] Bioengineering Group, Ri.MED Foundation, Palermo, Italy
[b] Department of Engineering, University of Palermo, Palermo, Italy
[c] UCL Institute of Cardiovascular Science& Great Ormond Street Hospital for Children, London, United Kingdom
[d] UCL Mechanical Engineering, University College London, London, United Kingdom

ARTICLE INFO

Keywords:
Atrial fibrillation
Left atrial appendage
Fluid-structure interaction
Cardiovascular engineering
Patient-specific numerical models

ABSTRACT

Background: Complications of atrial fibrillation (AF) include ischemic events originating within the left atrial appendage (LAA), a protrusion of the left atrium with variable morphological characteristics. The role of the patient specific morphology and pathological haemodynamics on the risk of ischemia remains unclear.
Methods: This work performs a comparative assessment of the hemodynamic parameters among patient-specific LAA morphologies through fluid-structure interaction computational analyses. Three LAA models per each of the four commons patient-specific morphological families (*chicken wing, cactus, windsock*, and *cauliflower*) were analysed. Mechanical properties of the tissue were based on experimental uniaxial tests on a young pig's heart. Boundary conditions were imposed based on clinical assessments of filling and emptying volumes. Sinus rhythm and atrial fibrillation operative conditions were simulated and analysed.
Results: For each model, the effect of morphological and functional parameters, such as the number of trabeculae and LAA stroke volume, over the hemodynamics established into the appendage was analysed. Comparison between results obtained in healthy and diseased conditions suggested the introduction of a new parameter to quantify the risk of thrombosis, here called *blood stasis factor* (BSF). This is defined as the LAA surface area which permanently experiences levels of shear strain rate inferior to a threshold value, set to 5 s^{-1} (BSF5).
Conclusions: This work suggests that the current morphological classification is unsuitable to evaluate the probability of thrombus formation. However, hemodynamic parameters easy to determine from clinical examinations, such as normalised stroke volume, LAA orifice flow rate and presence of extensive trabeculations can identify departures from healthy hemodynamics in AF and support a more systematic stratification of the thromboembolic risk.

1. Introduction

Atrial fibrillation (AF) is a pathology that affects the heart rhythm and is directly related to the increase in thromboembolic risk and ischemic events [1,2]. AF occurs when the electrical activity in the atria becomes disorganised due to the activation of several trigger points on the atrial walls, causing very fast and irregular contractions [3]. Over 90 % of thrombi involving ischemic events due to not valvular atrial fibrillation are reported to originate in the left atrial appendage (LAA) [4,5].

The LAA is an anatomical structure protruding from the left atrium which is believed to act as a decompression chamber of the left atrium during ventricular systole [6], and helps to normalise atrial pressure through the release of natriuretic peptide [7]. The LAA shape is largely variable between individuals [8], and is commonly classified into four morphological groups, identified as *chicken wing, cactus, windsock* and *cauliflower* (here reported from the most to the least common observed in patients) [9].

* Corresponding author at: UCL Mechanical Engineering, University College London, Torrington Place, London WC1E 7JE, United Kingdom.
E-mail address: g.burriesci@ucl.ac.uk (G. Burriesci).
[1] These authors contributed equally to this work.

https://doi.org/10.1016/j.cmpb.2024.108056
Received 16 December 2023; Received in revised form 28 January 2024; Accepted 1 February 2024
Available online 2 February 2024

Although the correlation between AF and the formation of thrombi in the LAA is well established [10,11], the role of LAA morphology with thromboembolic risk remains unclear [12,13], despite being widely investigated. A number of computational fluid dynamics (CFD) studies based on patient-specific LAA models have analysed the haemodynamic effects of AF [10,14,15]. The role of the LAA contractility and the effects produced by the chronicity of the pathology, such as volumetric remodelling, were also analysed on idealised LAA geometries [16] and on patient-specific models, by means of fluid-structure interaction (FSI) simulations [17]. These studies have suggested a correlation between anatomical phenotypes and the probability of clot formation, although they were not designed to identify a direct association between the morphological class and the risk of thrombosis.

In this work, three patient-specific LAA computational models per each of the four common morphological classes (12 models in total) were analysed and compared under healthy and pathological operating conditions, with the aim to identify potential correlations between anatomical and functional LAA parameters and the probability of thrombus formation, so as to implement an appropriate methodology for thromboembolic risk stratification applicable to common clinical practice. The study aims to identify fluid-dynamics parameters directly responsible for the clot formation that may support the clinical assessment of the thromboembolic risk through basic clinical measurements.

2. Methods

2.1. Models design

Three LAA patient-specific models were considered for each morphological family (3 × *chicken wing*, 3 × *cactus*, 3 × *windsock* and 3 × *cauliflower*), for a total of twelve models. These models were acquired by computed tomography scans of adult population not affected by AF, and classified by expert cardiologists. The acquired volumes represent the blood content within the LAA at the beginning of the filling phase and the adjacent anatomical part, such as the left atrium and pulmonary veins. Patients provided written informed consent to participate in the study, according to the recommendations of the South East Research Ethics Research Committee, Aylesford, Kent, United Kingdom. For each model, only the LAA region was analysed, with the aim to better isolate the effect of the LAA, as suggested in previous studies from our group [16,17]. The models, represented in Fig. 1, were created following the procedure described in detail in Musotto et al. [17]. In brief, the LAA surface and a portion of the atrium terminating halfway between the proximal section of the LAA neck and the pulmonary veins was extracted for each model. This surface was closed with a bulge at the open inlet to define the fluid domain. The surface was also used as the inner wall of the solid structure, obtaining the outer wall by offsetting the same surface by 2.1 mm [18], after smoothening it to remove discontinuities due to the presence of trabeculations [17]. The geometries of the fluid domain and solid structure were then imported in the commercial software *Ansys 2022 R2* for meshing and performing FSI simulations. In particular, a mesh of tetrahedral elements was employed for both fluid and structural domains, with a density of 70 elements per cubic millimetre, whose accuracy was already verified in Musotto et al. [17]. The structural domain was solved through the *Transient Structural* module, while the fluid domain was analysed through the *CFX* package. The FSI calculation was performed with the *System Coupling* module available on ANSYS Workbench [19], using a one-way approach.

This is far more efficient in terms computational resources than the two-way approach, albeit less accurate in fully capturing the interaction between the fluid and structural domains [20]. Still, variations between the two approaches on the relevant results (i.e. the estimated volume variation and velocity distributions) differ well below one order of magnitude. This was verified for model *chicken wing 1*, as reported in APPENDIX. This model was selected because the chicken wing morphology is reported to be by far the most common (observed in about half of patients) [9], and the morphology of model *chicken wing 1* was identified by three experienced cardiologists as the most representative of this class among the analysed shapes.

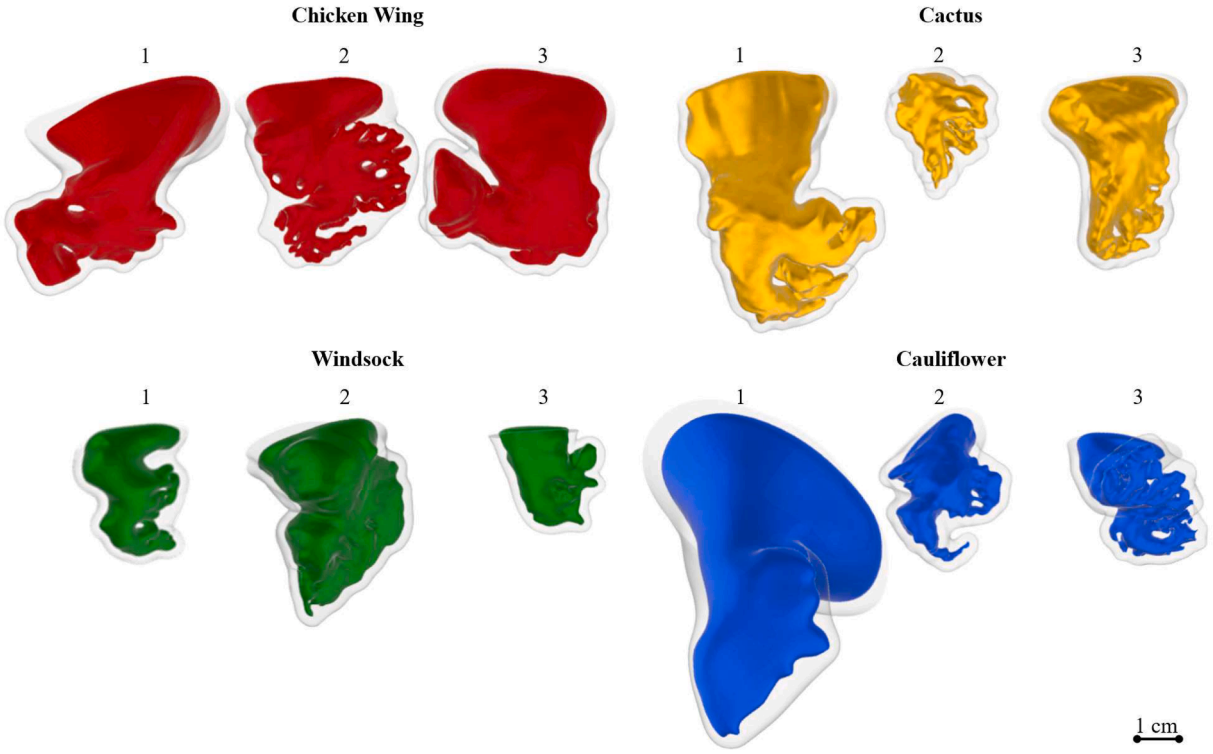

Fig. 1. LAA models classified by morphological families: *chicken wing* in red; *cactus* in yellow; *windsock* in green and *cauliflower* in blue.

2.2. Mechanical and rheological properties

The mechanical response of the LAA tissue was obtained from uniaxial mechanical tests performed on anatomical sections taken from a young pig heart harvested from a local slaughter house. Tests were carried out on fresh tissue, within few hours from the animal death, to minimise sample deterioration. Mechanical tests were performed on a Zwickyline uniaxial universal testing machine (Zwick.Roell GmbH & Co, Ulm, Germany) with a 500 N loadcell. Three rectangular specimens were prepared, with a width of 7 mm, imposing an initial gauge length of 12 mm. The average thickness of each specimen was measured with a Mitutoyo gauge micrometre (Mitutoyo Corporation, Tokyo, Japan), performing five measurements at evenly spaced locations along the specimen axis, covering the entire gauge length.

Tensile tests were performed keeping the specimens immersed in a phosphate-buffered saline solution at body temperature (37 °C), imposing a crosshead speed of 1 mm/s until failure. Nominal stress and strain were recorded during the whole test.

Fig. 2a reports the stress-strain curves measured for the three specimens (black lines). Two of the three specimens (2 and 3 indicated in the plot with dashed and dotted black lines, respectively) failed before passing the toe typically observed in biological soft tissues [18]. This was expected, especially for the LAA appendage tissue, whose characterisation is affected by the complex topological and microstructural features captured in each specimen [18], which results into high variability in the tissue mechanical properties. Still, specimen 1 (indicated as continuous black line) reached the breaking point at substantially larger values of stress and strain than the others, well capturing the typical stress-strain nonlinearity expected in biological soft tissues. Hence, this curve was selected to characterise the models' material, and fitted with a third order Ogden model [21,22]. The fitting curve is plotted in Fig. 2a as a dashed red line.

In particular, Ogden constitutive representation was selected as it is suitable to describe the behaviour of biological soft tissues, including cardiac muscles [23], and is reported to be able to well replicate the physiological pressure-volume response of myocardial tissue [24]. The model is described in Eq. (1):

$$W_{Ogden} = \sum_{i=1}^{3} \frac{\mu_i}{\alpha_i} J^{\frac{-\alpha_i}{3}} \left(\lambda_1^{\alpha_i} + \lambda_2^{\alpha_i} + \lambda_3^{\alpha_i} - 3\right); \quad (1)$$

where J is the Jacobian measuring dilatancy, λ_1, λ_2, and λ_3 are the principal stretches, $\mu_i$are related to the shear modulus, and $\alpha_i$are material constants. The Ogden constants best fitting the selected stress-strain curve were $\mu_1 = 0.05$, $\mu_2 = 0.175101419$, $\mu_3 = -0.217898141$, $\alpha_1 = 8.031219931$, $\alpha_2 = 7.015481171$, $\alpha_3 = 7.336946763$. The third order model was used because it guarantees satisfactory fitting with the experimental curves (resulting in residual equal to $4.4\ 0{\cdot}10^{-6}$).

Moreover, this curve allowed to obtain a good matching with the stroke volume of the LAA reported in clinical data under physiological loading conditions [25].

At the scale of the study, human blood can be considered a homogeneous non-Newtonian fluid with shear thinning, thixotropic and viscoelastic properties [26–28]. A number of rheological relations have been developed to describe this behaviour [29], mostly based on the visco-plastic rheological model implemented by Casson [30]. However, these are designed to simulate steady-state conditions [31], and can therefore result in overestimation of the viscosity and blood stasis [17]. Hence, it was preferred modelling blood as a Newtonian fluid, with density of 1062 kg/m^3 and dynamic viscosity of 0.0037 Pa·s. This assumption, which leads to conservative results in the assessment of thromboembolic risk [17,32] and reduces the computational cost of the analyses, does not introduce significant differences in the results, as verified by a comparison with the Casson model performed for one of the configurations (*chicken wing 1*) and reported in the APPENDIX.

2.3. Boundary conditions

Two operative conditions were analysed: sinus rhythm (which represents the healthy condition) and acute AF. The sinus rhythm condition was simulated imposing a pressure curve measured in the atrium on patients without atrial fibrillation [33], considering a heart frequency of 70 bmp (continuous black line in Fig. 2b).

In the sinus rhythm operative condition, the contractile action of the LAA was modelled using the procedure described in Musotto et al. [17], which allows to realistically simulate the active contraction of the LAA through a virtual thermal load. In particular, coefficients of thermal expansion $C_x = C_y = 0.03$ were used in the LAA wall plane, and a coefficient $C_z = -0.06$ across the wall thickness, so as to model the incompressibility of the muscle during contraction. A spatially uniform thermal load (represented as dashed black lines in Fig. 2b,c) was applied to all wall elements, following in time a curve suitably calibrated to obtain, in combination with the pressure load, similar physiological volume variation as reported for the LAA at the emptying and filling phases by Li et al. [34]. Since models were obtained from radiological acquisitions and are therefore representative of LAAs subjected to physiologically pressurised conditions, an additional constant thermal load was tuned to restore the initial volume at the beginning of the filling phase (selected also as a reference for the beginning of the cardiac cycle). The tuning of the thermal load (curve and thermal expansion coefficients) was performed on the *chicken wing 1* morphology, replicating the volume variation curve, both in shape and magnitude, as described by Li et al. [34]. As mentioned above, between the analysed anatomies, this model is the most representative of the most common morphological class [5,9]. The resulting thermal curve (based on an arbitrary reference temperature variation $\Delta T = 0.9$ °C) is plotted in Fig. 2b as a dashed black line. The pressure and thermal curves (Fig. 2b) were applied to all models to simulate sinus rhythm condition.

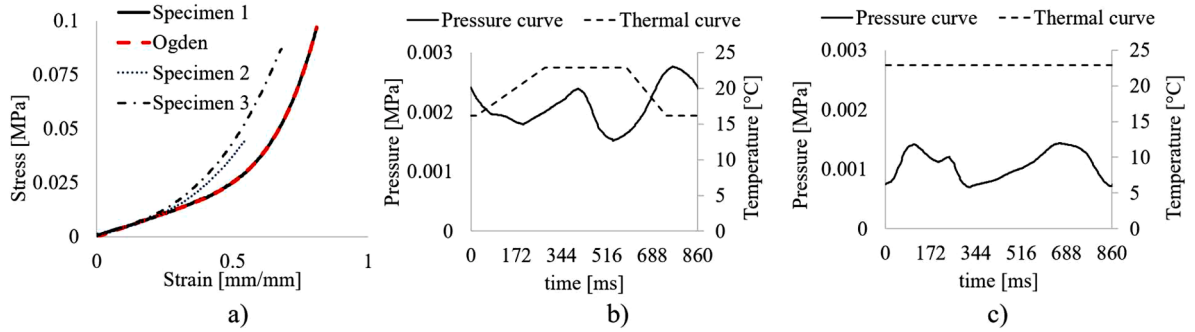

Fig. 2. (a) Stress-strain curve resulting from the uniaxial mechanical tests on LAA tissue for specimens 1,2 and 3 (continuous, dashed and dotted black lines, respectively), and Ogden fitting curve on the selected specimen 1 (dashed red line); (b) boundary conditions used to simulate sinus rhythm; and (c) boundary conditions used to simulate atrial fibrillation conditions.

In order to model AF condition, the pressure curve reported by Park et al. [35], based on clinical measurements in patients with atrial fibrillation, was employed (continuous black line Fig. 2c). In the pathological condition, the thermal component associated with the active contraction was not included, as this is negligible during AF [8]. As a result, a constant thermal load corresponding to that replicating the phase of maximum filling that the LAA reaches in the condition of sinus rhythm (T_{max} = 0.9 °C) was applied (dashed black line in Fig. 2c). Therefore, the filling and emptying phases in AF are passive, and regulated only by the compliance of the LAA wall under the action of the applied pressure.

Due to the one-way approach used in the FSI numerical model, the

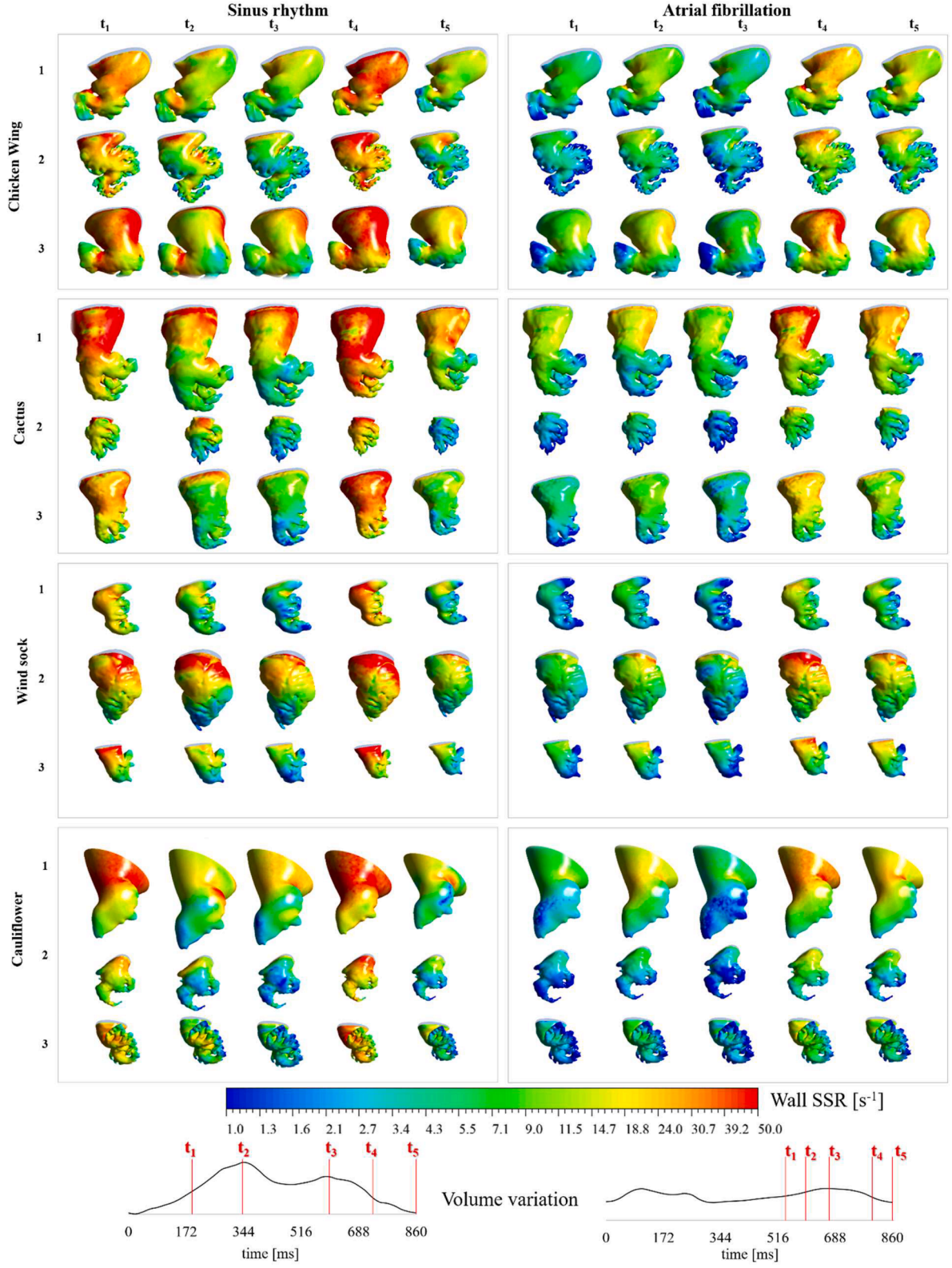

Fig. 3. Wall SSR in sinus rhythm at five-time instants computed for the last simulated cardiac cycle.

pressure curve was directly imposed on the internal walls of the structural domain.

Simulations were run for 2 consecutive cardiac cycles, verifying that the end of the second cycle was identical to the end of the first one for all simulations. As this confirmed that the whole second cycle has already reached periodicity, this was considered for the results analysis.

2.4. Statistical analysis

A parameter commonly used in clinical practice to evaluate the thromboembolic risk is the velocity at the LAA orifice [36–39]. Hence, in order to confirm the relevance of this quantity, the mean velocity at the orifice, u_{mean}, was estimated for all models. Also, other parameters that can be clinically measured and serve for diagnostic support were quantified and evaluated in terms of their relation with the risk of thrombosis, by means of linear regression and statistical analysis.

In summary, the clinically measurable quantities investigated were:

- mean velocity at the LAA orifice, u_{mean};
- LAA volume at the maximum expansion, V_{max};
- LAA volume at the maximum contraction, V_{min};
- LAA stroke volume, $\Delta V = V_{max} - V_{min}$;
- normalised stroke volume, $V^* = \Delta V / V_{min}$;

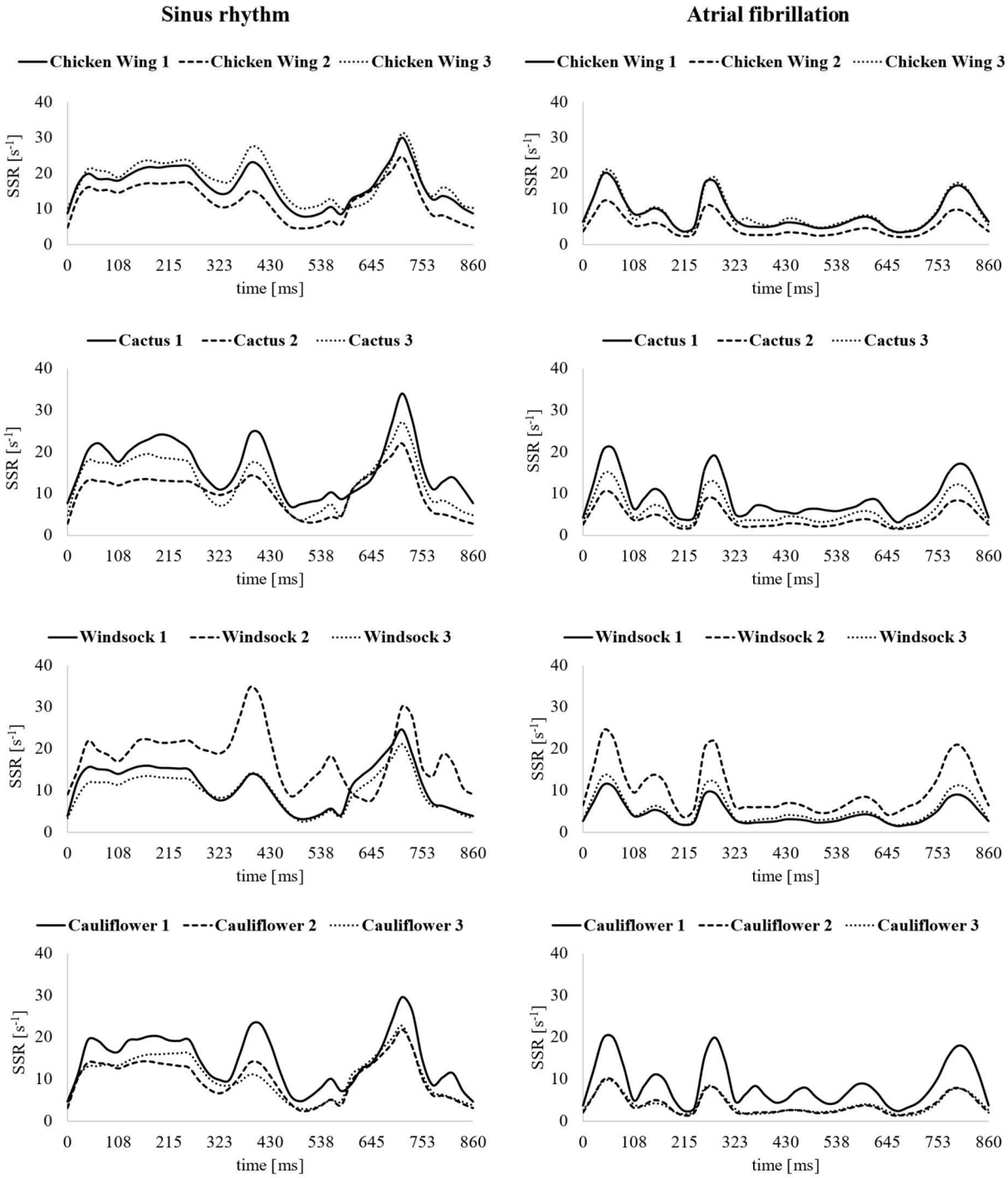

Fig. 4. Average wall SSR for the four morphological classes in sinus rhythm and atrial fibrillation conditions.

In addition, to consider the role of local topological features, the number of trabeculae, $N_{trabeculae}$, was also evaluated.

3. Results

For better clarity of representation, and in order to enlighten the potential role of current LAA classification, results are grouped based on the morphological classes (*chicken wing, cactus, windsock* and *cauliflower*).

Shear Strain Rate (SSR) was chosen as the physical parameter to analyse the probability of clot formation.

In fact, low levels of SSR are associated with blood stasis [40–42] and are often employed in computational analyses to assess the risk of thrombosis [17,41,42]. Contour maps of the wall SSR values, obtained in the different models at five representative instants of the cardiac cycle (t_1, t_2, t_3, t_4 and t_5), are represented in Fig. 3. In particular, the time instants were selected on the basis of the typical volume variation curves for sinus rhythm and AF (represented at the bottom of Fig. 3): t_1 is selected in the middle of the expansion curve; t_2 corresponds to the instant of maximum filling; t_3 is the beginning of the atrial contraction (active in the case of sinus rhythm and passive for AF); t_4 is selected in the middle of the contraction curve; and t_5 is the instant when the LAA volume is minimum. A logarithmic rainbow colour scale was selected to better highlight the variations of the wall SSR.

The evolution in time of the SSR averaged over the blood-structure wall interface for the different models is reported in Fig. 4. These values are calculated on the LAA surface, excluding the atrial portion of the domain (proximally to the end of the LAA neck).

It is worth mentioning that, based on the Virchow triad, clot formation is most likely to initiate at the walls, where abnormal blood flow can interact with potentially injured tissues [43,44]. Hence, a parameter is defined here and used in the reminder of this paper to quantify the thrombosis risk, indicated as *blood stasis factor* (BSF). This corresponds to the LAA area permanently exposed to a wall SSR below 5 s^{-1} (BSF5). This threshold value was assumed indicative of unphysiological conditions because it corresponds to the minimum BSF computed in all models when subjected to healthy sinus rhythm conditions. This can be appreciated looking at the histogram in Fig. 5, where red bars indicating the LAA areas below 5 s^{-1} for all models are not observable in sinus rhythm condition. To identify higher propensity towards unphysiological stagnation during healthy operating conditions, areas permanently exposed to a wall SSR below 10 s^{-1} (BSF10) are also quantified and represented as yellow bars in Fig. 5.

Regions where BSF5 and BSF10 were observed are represented in Fig. 6 as red (high risk regions) and yellow (moderate risk regions) contour maps, respectively. Blue areas represent the regions where SSR value becomes larger than 10 s^{-1} at least for some part of the cardiac cycle.

Correlation of BSF with the common morphological classification and with global hemodynamic parameters was investigated by means of linear regression analysis and statistical tests.

Anova test indicated that BSF5 does not exhibit any statistical difference among the four morphological classes analysed (p-value = 0.365).

Univariable linear regression analysis was applied to evaluate the suitability of the other clinically measurable quantities (reported in Table 1) to serve as predictor of the thromboembolic risk.

In particular, T-test was used to determine if the relationship is statistically significant, and R-squared was employed to estimate the fraction of BSF5 variance explained by the predictor [45].

Pearson correlation was computed between BSF5 and all the selected variables, estimated in AF conditions. All variables were normalised in the range [0,1], to ease comparison between the computed regression coefficients.

In Table 2, all computed values are ordered for decreasing values of R-squared.

4. Discussion

Associations of current morphological classification with the thromboembolic risk is still debated [9,39,46,47]. Di Biase et al. [9] reported that patients with non-*chicken wing* LAA morphology were more likely to experience embolic events than those with *chicken wing* type. Lee et al. [39] suggested that LAA morphology was related to strokes and this relationship is partially associated with the change in size and flow velocity of the different LAA. In particular, they confirm decreased stroke risk for the *chicken wing* type, reporting an increased risk for the *cauliflower* type. Ren et al. [46] question current morphological classification, that is considered complex and confusing, whilst in their opinion essentially all LAA morphologies can be classified as windsock-like. Koskinas et al. [47] support the importance of LAA anatomic variability, especially to clinical and percutaneous procedure evaluation.

The present study indicates no direct relationship between the common morphological class and fluid-dynamic conditions that can be associated with thrombosis (estimated on the basis of the wall SSR and BSF5). This is evident in Fig. 4, where the average wall SSR trend during the cardiac cycle is compared for models of the same class, both in sinus rhythm and AF conditions. In the 12 cases simulated in this analysis, the intra- and inter-class variabilities are comparable.

Contour maps represented in Fig. 3 suggest that the presence of trabeculae, lobes and knees are associated with locally low values of SSR, especially in AF condition, with consequently higher propensity towards clot formation.

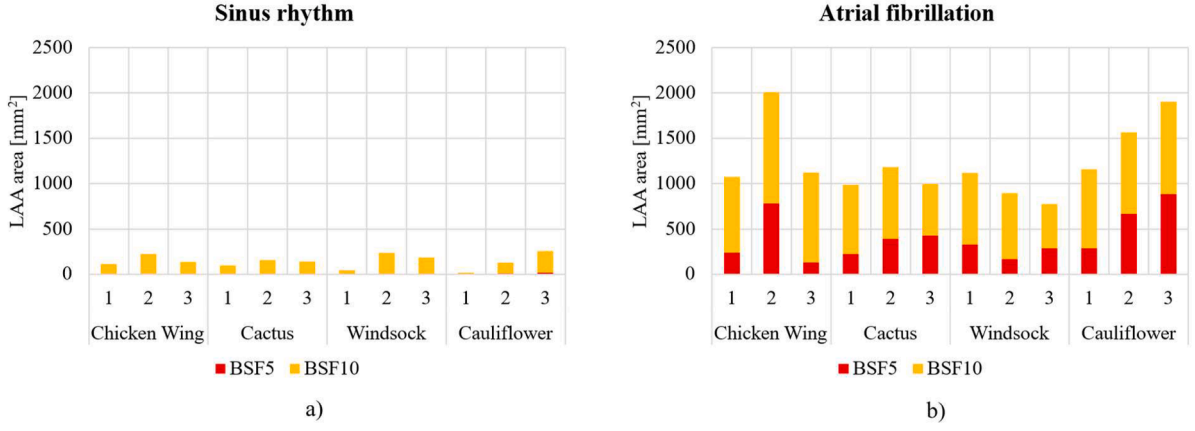

Fig. 5. BSF values. (a) Sinus rhythm condition; (b) atrial fibrillation condition.

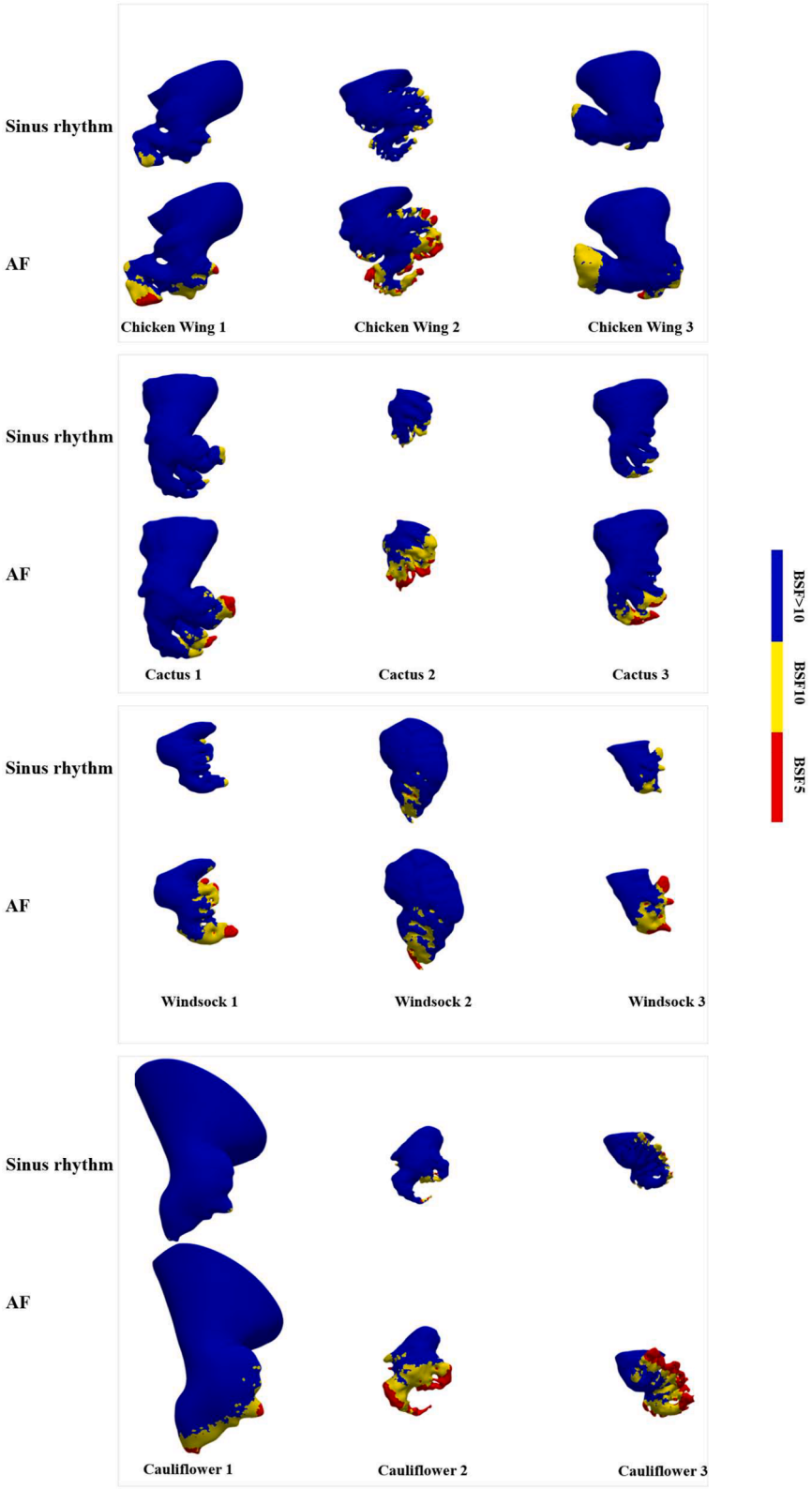

Fig. 6. Risk maps. BSF5: red (high risk regions); BSF10: yellow (moderate risk regions); BSF>10: blue (low risk regions).

Fig. 5 clearly indicates that the presence of regions with SSR permanently below 5 s^{-1} (BSF5) discriminates between healthy and pathological conditions, with sinus rhythm conditions securing in all cases some cyclic washing flow. In sinus rhythm, small BSF10 regions (5 s^{-1} < SSR < 10 s^{-1}) are observed in all models, although their extension is not always correlated with a corresponding risk in AF.

The distribution of red areas (BSF5) in Fig. 6 confirms an association with the presence of lobes and, in particular, with trabeculations. The figure also shows that the initial LAA volume in the AF simulations enlarges compared to that in sinus rhythm. In fact, as under pathological

Table 1
Mean velocity at the LAA orifice (u_{mean}), LAA volume at the maximum expansion (V_{max}), LAA volume at the maximum contraction (V_{min}), LAA stroke volume (ΔV), normalised volume (V^*), LAA flow rate (Q), normalised flow rate (Q^*) in atrial fibrillation condition. The values within parentheses are related to the corresponding sinus rhythm condition.

Morphologies	u_{mean} [cm/s]	V_{max} [mm^3]	V_{min} [mm^3]	ΔV [%]	V^* [-]	Q [cm^3/s]	Q^* [1/s]
Chicken Wing 1	6.9 (8.9)	6260 (8824)	4990 (3506)	85 (161)	0.25 (1.52)	20.6 (33.9)	0.33 (0.38)
Chicken Wing 2	4.7 (7.9)	5530 (7073)	4670 (3030)	58 (102)	0.18 (1.33)	13.5 (26.0)	0.24 (0.37)
Chicken Wing 3	7.6 (10.9)	9150 (13,400)	7270 (5390)	89 (176)	0.26 (1.49)	30.5 (55.0)	0.33 (0.41)
Cactus 1	9.4 (16.0)	8740 (13,057)	7060 (4781)	69 (153)	0.24 (1.73)	27.0 (60.5)	0.31 (0.46)
Cactus 2	3.5 (6.5)	1930 (2276)	1700 (1096)	42 (68)	0.14 (1.08)	3.6 (7.2)	0.19 (0.31)
Cactus 3	4.6 (8.0)	4170 (5589)	3460 (2204)	22 (118)	0.21 (1.54)	11.7 (24.9)	0.28 (0.44)
Windsock 1	3.3 (7.1)	2248 (2768)	1939 (1173)	49 (83)	0.16 (1.36)	4.9 (12.2)	0.22 (0.44)
Windsock 2	8.2 (13.1)	124,632 (1757)	9992 (8486)	95 (175)	0.25 (1.07)	40.8 (75.5)	0.33 (0.43)
Windsock 3	4.5 (7.1)	1814 (2218)	1530 (985)	71 (109)	0.19 (1.25)	4.5 (8.0)	0.25 (0.36)
Cauliflower 1	8.1 (11.1)	9339 (1399)	7323 (4706)	91 (186)	0.28 (1.97)	32.1 (66.5)	0.34 (0.48)
Cauliflower 2	3.1 (5.6)	3321 (4040)	2914 (1980)	41 (71)	0.14 (1.04)	6.6 (12.9)	0.20 (0.32)
Cauliflower 3	3.7 (8.1)	2435 (2930)	2137 (1310)	41 (70)	0.14 (1.24)	5.1 (12.8)	0.21 (0.44)

Table 2
Linear regression models and statistical results showing the correlation between the BSF5 factor and clinically measurable variables. All measures are evaluated in atrial fibrillation conditions. Rows are ordered from decreasing values of R-squared. Bold values indicate significative p-values.

	Pearson Correlation	Regression Coefficient	R-squared [%]	P-value (*t*-test)
$N_{trabeculae}$	0.8182	0.838	66.95	**0.0011**
V^*	−0.7159	−0.6538	51.25	**0.0088**
Q^*	−0.6739	−0.5917	45.42	**0.0162**
u_{mean}	−0.6537	−0.602	42.73	**0.0211**
Q_{mean}	−0.5916	−0.551	35	**0.0427**
ΔV	−0.591	−0.5404	34.93	**0.043**
V_{max}	−0.5311	−0.5162	28.2	0.0756
V_{min}	−0.4855	−0.4833	23.57	0.1096

conditions the active atrial contraction is impaired, the muscle remains relaxed and can only expand under the effect of the physiological pressure. In the long-term, such mode of deformation might be a factor contributing to the remodelling of the LAA observed in persistent AF.

Statistical analysis validates the use of the blood velocity at the LAA orifice as a good predictor of BSF5 (p-value = 0.0211, R-squared = 43%).

However, the number of trabeculae, N, and the normalised stroke volume, V^*, exhibit improved regression coefficients and increased R-squared (respectively 0.83 and 67% for N, −0.65 and 51% for V^*), resulting better predictors (respectively p-value < 0.01) than the LAA ostium velocity. The number of trabeculae has the highest prediction power (p-value = 0.0011), along with the normalised stroke volume in AF condition (p-value = 0.0088). These two parameters, albeit independent (Pearson Correlation < 0.5, R-squared = 0.23, p-value > 0.05), represent two different forms of fluid-dynamics impairment. Trabeculations, in normal conditions, are expected to participate to the LAA contractile dynamics. However, when active contraction is lost, they act as flow resistances, reducing at the same time the local compliance of LAA by constraining the opposite appendage wall that they connect. Hence, they can be seen as a descriptor of 'local' reduction in the washout flow. Similarly, lower normalised stroke volumes are associated with reduced flowrates entering and leaving the LAA, providing a 'global' indication on the blood cleansing in the appendage.

The independency of these two parameters also allows their combination to further improve the risk prediction, with the ratio N/V^* (number of trabeculae divided by normalised stroke volume) providing an effective indication of the BSF5 (p-value $\langle$ 0.001, R-squared $\rangle$ 74% and Pearson correlation $>$ 86 %).

Although this work improves the comprehension of the phenomenon, some limitations have to be highlighted. In particular, mechanical characterisation of the tissue response was based on a single test performed on one pig's heart. Also, the LAA wall thickness was assumed uniform and identical for all models, and the muscle anisotropy was neglected. Blood was modelled as a Newtonian fluid. Although this assumption is widely adopted, it does not capture the expected increase of viscosity in the stagnation regions, resulting in a potential underestimation of the thromboembolic risk. The absence of direct pressure measurements for each patient necessitated the adoption of standardised boundary conditions for the twelve models representing both sinus rhythm and atrial fibrillation. As discussed in the methods section, calibration of the boundary conditions was conducted using a single model and subsequently applied to all twelve models. Still, this procedure allows the comparability of the models by isolating their morphological features and ensuring the reproducibility of the methodology. One-way FSI analyses were performed, assuming that the effect of the blood shear stress on the tissue deformation is negligible. Finally, in order to translate this model in the clinical practice, we anticipate that validation versus retrospective data will be performed.

5. Conclusions

This work analyses twelve patient-specific models belonging to different morphological classes to investigate the correlation between morphological and hemodynamic parameters and the thromboembolic risk in atrial fibrillation. The study is conducted by means of FSI numerical simulations, comparing the flow distribution associated with sinus rhythm and atrial fibrillation conditions.

A new parameter is identified as descriptive of abnormal levels of stagnation occurring during AF, and hence proposed to quantify the thrombosis risk. This, indicated as BSF5, is defined as the LAA surface area which permanently experiences levels of shear strain rate inferior to a threshold value set to 5 s^{-1}.

The study suggests that the common morphological classification and the LAA volume have no direct association with the risk, whilst blood velocities at the LAA orifice are acceptable risk indicators.

Still, regression and statistical analysis suggests that trabeculations and the normalised stroke volume have a more direct correlation with the risk, with their ratio providing a very good estimate.

Introduction of these parameters descriptive of hemodynamic alterations aside current clinical criteria such as the $CHADS_2$ and CHA_2DS_2-VASc score, may improve stratification and support more informed clinical decisions.

CRediT authorship contribution statement

Giulio Musotto: Writing – original draft, Software, Methodology, Formal analysis, Data curation, Conceptualization. **Alessandra Monteleone:** Writing – original draft, Software, Methodology, Formal analysis, Data curation, Conceptualization. **Danila Vella:** Writing –

original draft, Methodology, Data curation, Conceptualization. **Bernardo Zuccarello:** Supervision, Conceptualization. **Ruggero Cannova:** Data curation. **Andrew Cook:** Data curation. **Giorgia Maria Bosi:** Methodology, Data curation. **Gaetano Burriesci:** Writing – review & editing, Supervision, Methodology, Formal analysis, Conceptualization.

Declaration of competing interest

The authors declare that they have no known competing financial interests or personal relationships that could have appeared to influence the work reported in this paper.

Appendix

FSI analysis details

In this section, a comparison between one-way and two-way FSI approaches is reported. In particular, FSI partitioned analysis involves two separated domains for the structure and the fluid which are separated through FSI interfaces. Each domain is analysed through a specialised solver, whilst at the interfaces, solutions are shared. Two different FSI approaches can be distinguish: one-way and two-way. The one-way technique involves a unidirectional analysis where only the information of the structural domain (updated nodes positions and velocities) is shared with the fluid domain. On the other hand, the two-way approach is a bidirectional analysis, based on the mutual exchange of information between structural and fluid domains.

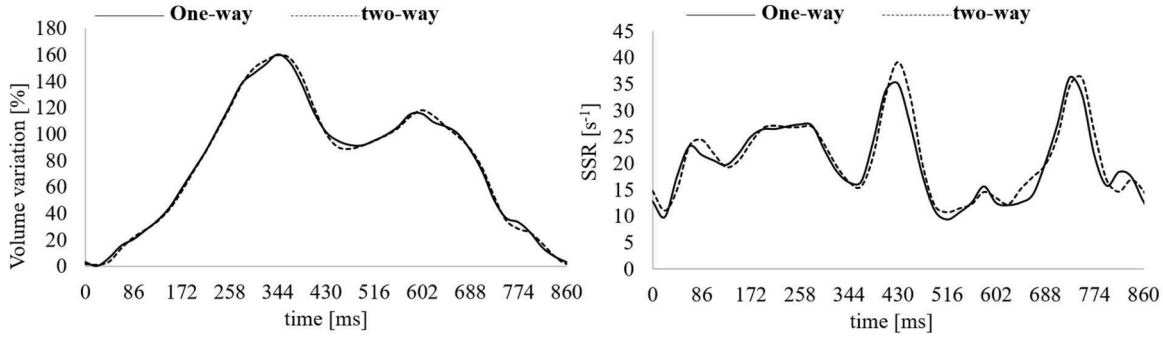

Fig. A1. Comparison between one-way (continuous line) and two-way (dashed line) approaches.

Fig. A1 shows a comparison between one-way (black continuous line) and two-way (dashed black line) FSI approaches applied to the *chicken wing 1* model. In particular, the volume variation and the shear strain rate (SSR) were compared using the two schemes. Since there are no significative differences between the two techniques, one-way was chosen to perform simulations which allow to reduce computational efforts and calculation times.

Fluid model details

In this section a comparison between Newtonian and Casson models is reported.

Although the rheological properties of blood exhibit a typical shear thinning behaviour, in this study the fluid was modelled as Newtonian. In order to verify the influence of this assumption, a non-Newtonian model typically used to describe the blood behaviour, the Casson model, was used for comparison. The fluid properties used to perform the simulations with the Newtonian and Casson models are reported in Table A1. Fig. A2 shows the comparison between Newtonian (continuous black line) and Casson (dashed black line), analysing the LAA volume variation and SSR. Since no relevant differences were noted and the Newtonian model allows to obtain more conservative results in terms of thromboembolic risk, the latter was used in the simulations.

Table A1
Fluid properties for Newtonian and Casson models.

Option	Newtonian model	Casson model
Yield Stress	–	0.0038 [Pa]
Viscosity Consistent	–	0.0042 [Pa s]
Density	1060 [Kg/m^3]	1060 [Kg/m^3]
Dynamic Viscosity	0.0037 [Pa s]	–

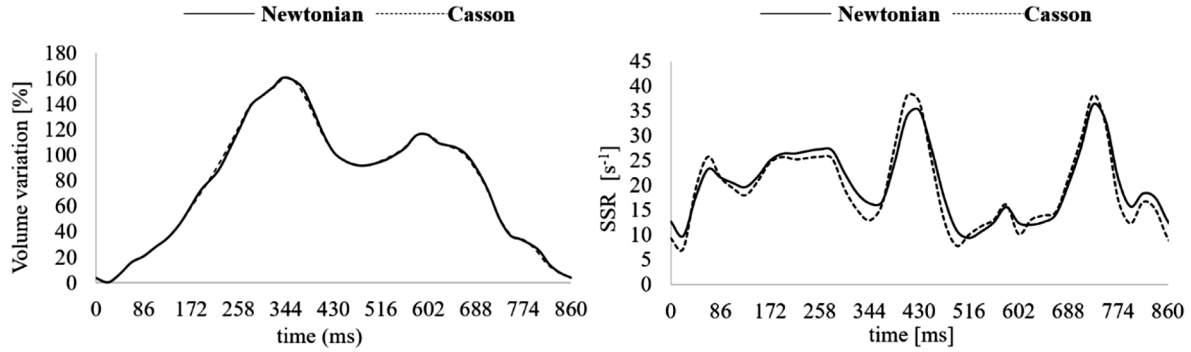

Fig. A2. Comparison between Newtonian (continuous line) and Casson (dashed line) models in terms of volume variation and SSR.

References

[1] Y. Hagiwara, H. Fujita, S.L. Oh, J.H. Tan, R.S. Tan, E.J. Ciaccio, U.R. Acharya, Computer-aided diagnosis of atrial fibrillation based on ECG signals: a review, Inf. Sci. 467 (2018) 99–114, https://doi.org/10.1016/j.ins.2018.07.063 (N Y).

[2] S. Nattel, New ideas about atrial fibrillation 50 years on, Nature 415 (2002) 219–226, https://doi.org/10.1038/415219a.

[3] G.W. Petty, R.D. Brown, J.P. Whisnant, J.D. Sicks, W.M. O'Fallon, D.O. Wiebers, Ischemic stroke subtypes, Stroke 30 (1999) 2513–2516, https://doi.org/10.1161/01.STR.30.12.2513.

[4] F. Joseph L, M.D. Blackshear, J.A. Odell, Appendage obliteration to reduce stroke in cardiac surgical patients with atrial fibrillation, Soc. Thorac. Surg. 9 (61) (1996) 755.

[5] D.R. Holmes, K. Korsholm, J. Rodés-Cabau, J. Saw, S. Berti, M.A. Alkhouli, Left atrial appendage occlusion, EuroIntervention 18 (2023) e1038–e1065, https://doi.org/10.4244/EIJ-D-22-00627.

[6] N.M. Al-Saady, O.A. Obel, A.J. Camm, Left atrial appendage: structure, function, and role in thromboembolism, Heart 82 (1999) 547–554, https://doi.org/10.1136/hrt.82.5.547.

[7] T. Tabata, Relationship between left atrial appendage function and plasma concentration of atrial natriuretic peptide, Eur. J. Echocardiogr. 1 (2000) 130–137, https://doi.org/10.1053/euje.2000.0019.

[8] S. Yaghi, C. Song, W.A. Gray, K.L. Furie, M.S.V. Elkind, H. Kamel, Left atrial appendage function and stroke risk, Stroke 46 (2015) 3554–3559, https://doi.org/10.1161/STROKEAHA.115.011273.

[9] L. Di Biase, P. Santangeli, M. Anselmino, P. Mohanty, I. Salvetti, S. Gili, R. Horton, J.E. Sanchez, R. Bai, S. Mohanty, others, Does the left atrial appendage morphology correlate with the risk of stroke in patients with atrial fibrillation?: results from a multicenter study, J. Am. Coll. Cardiol. 60 (2012) 531–538.

[10] G.M. Bosi, A. Cook, R. Rai, L.J. Menezes, S. Schievano, R. Torii, G. Burriesci, Computational fluid dynamic analysis of the left atrial appendage to predict thrombosis risk, Front. Cardiovasc. Med. 5 (2018), https://doi.org/10.3389/fcvm.2018.00034.

[11] S. Han, M. Liu, R. Jia, Z. Cen, R. Guo, G. Liu, K. Cui, Left atrial appendage function and structure predictors of recurrent atrial fibrillation after catheter ablation: a meta-analysis of observational studies, Front. Cardiovasc. Med. 9 (2022), https://doi.org/10.3389/fcvm.2022.1009494.

[12] D.A. Lane, C.J. Boos, G.Y.H. Lip, Atrial fibrillation (chronic), 2014.

[13] S. Yaghi, A.D. Chang, R. Akiki, S. Collins, T. Novack, M. Hemendinger, A. Schomer, B.Mac Grory, S. Cutting, T. Burton, C. Song, A. Poppas, R. McTaggart, M. Jayaraman, A. Merkler, H. Kamel, M.S.V. Elkind, K. Furie, M.K. Atalay, The left atrial appendage morphology is associated with embolic stroke subtypes using a simple classification system: a proof of concept study, J. Cardiovasc. Comput. Tomogr. 14 (2020) 27–33, https://doi.org/10.1016/j.jcct.2019.04.005.

[14] A. Masci, L. Barone, L. Dedè, M. Fedele, C. Tomasi, A. Quarteroni, C. Corsi, The impact of left atrium appendage morphology on stroke risk assessment in atrial fibrillation: a computational fluid dynamics study, Front. Physiol. 9 (2019), https://doi.org/10.3389/fphys.2018.01938.

[15] L. Dedè, F. Menghini, A. Quarteroni, Computational fluid dynamics of blood flow in an idealized left human heart, Int. J. Numer. Methods Biomed. Eng. 37 (2021), https://doi.org/10.1002/cnm.3287.

[16] D. Vella, A. Monteleone, G. Musotto, G.M. Bosi, G. Burriesci, Effect of the alterations in contractility and morphology produced by atrial fibrillation on the thrombosis potential of the left atrial appendage, Front. Bioeng. Biotechnol. 9 (2021), https://doi.org/10.3389/fbioe.2021.586041.

[17] G. Musotto, A. Monteleone, D. Vella, S. Di Leonardo, A. Viola, G. Pitarresi, B. Zuccarello, A. Pantano, A. Cook, G.M. Bosi, G. Burriesci, The role of patient-specific morphological features of the left atrial appendage on the thromboembolic risk under atrial fibrillation, Front. Cardiovasc. Med. 9 (2022), https://doi.org/10.3389/fcvm.2022.894187.

[18] S. Javani, M. Gordon, A.N. Azadani, Biomechanical properties and microstructure of heart chambers: a paired comparison study in an ovine model, Ann. Biomed. Eng. 44 (2016) 3266–3283.

[19] S.K. Chimakurthi, S. Reuss, M. Tooley, S. Scampoli, ANSYS workbench system coupling: a state-of-the-art computational framework for analyzing multiphysics problems, Eng. Comput. 34 (2018) 385–411, https://doi.org/10.1007/s00366-017-0548-4.

[20] F.K. Benra, H.J. Dohmen, J. Pei, S. Schuster, B. Wan, A comparison of one-way and two-way coupling methods for numerical analysis of fluid-structure interactions, J. Appl. Math. 2011 (2011) 1–16, https://doi.org/10.1155/2011/853560.

[21] R. Ogden, Large deformation isotropic elasticity – on the correlation of theory and experiment for incompressible rubberlike solids, Proc. R. Soc. Lond. A Math. Phys. Sci. 326 (1972) 565–584, https://doi.org/10.1098/rspa.1972.0026.

[22] G.A. Holzapfel, R.W. Ogden, Constitutive modelling of passive myocardium: a structurally based framework for material characterization, Philos. Trans. R. Soc. A Math. Phys. Eng. Sci. 367 (2009) 3445–3475, https://doi.org/10.1098/rsta.2009.0091.

[23] M. Hadjicharalambous, R. Chabiniok, L. Asner, E. Sammut, J. Wong, G. Carr-White, J. Lee, R. Razavi, N. Smith, D. Nordsletten, Analysis of passive cardiac constitutive laws for parameter estimation using 3D tagged MRI, Biomech. Model. Mechanobiol. 14 (2015) 807–828, https://doi.org/10.1007/s10237-014-0638-9.

[24] R.W. Ogden, Nonlinear elasticity, anisotropy, material stability and residual stresses in soft tissue. Biomechanics of Soft Tissue in Cardio-Vascular Systems, Springer, 2003, pp. 65–108.

[25] C.Y. Li, B.L. Gao, X.W. Liu, Q.Y. Fan, X.J. Zhang, G.C. Liu, H.Q. Yang, P.Y. Feng, Y. Wang, P. Song, Quantitative evaluation of the substantially variable morphology and function of the left atrial appendage and its relation with adjacent structures, PLoS ONE 10 (2015) e0126818, https://doi.org/10.1371/journal.pone.0126818.

[26] A.J. Apostolidis, M.J. Armstrong, A.N. Beris, Modeling of human blood rheology in transient shear flows, J. Rheol. 59 (2015) 275–298, https://doi.org/10.1122/1.4904423.

[27] D.A. Fedosov, W. Pan, B. Caswell, G. Gompper, G.E. Karniadakis, Predicting human blood viscosity in silico, Proc. Natl. Acad. Sci. 108 (2011) 11772–11777, https://doi.org/10.1073/pnas.1101210108.

[28] S. Chien, Shear dependence of effective cell volume as a determinant of blood viscosity, Science 168 (1970) 977–979, https://doi.org/10.1126/science.168.3934.977.

[29] M.Y. Yilmaz, F. Gundogdu, A critical review on blood flow in large arteries; relevance to blood rheology, viscosity models, and physiologic conditions, Korea-Aust. Rheol. J. 20 (4) (2008) 197–211.

[30] N. Casson, A flow equation for pigment-oil suspensions of the printing ink type. Rheology of Disperse Systems Rheology of Disperse Systems, Pergamon Press, 1959, pp. 84–104.

[31] S. Jariwala, J.S. Horner, N.J. Wagner, A.N. Beris, Application of population balance-based thixotropic model to human blood, J Non-Newton. Fluid Mech. 281 (2020) 104294, https://doi.org/10.1016/j.jnnfm.2020.104294.

[32] A. Ducci, F. Pirisi, S. Tzamtzis, G. Burriesci, Transcatheter aortic valves produce unphysiological flows which may contribute to thromboembolic events: an *in-vitro* study, J. Biomech. 49 (2016) 4080–4089, https://doi.org/10.1016/j.jbiomech.2016.10.050.

[33] S. Nakatani, M.J. Garcia, M.S. Firstenberg, L. Rodriguez, R.A. Grimm, N. L. Greenberg, P.M. McCarthy, P.M. Vandervoort, J.D. Thomas, Noninvasive assessment of left atrial maximum dP/dt by a combination of transmitral and pulmonary venous flow, J. Am. Coll. Cardiol. 34 (1999) 795–801.

[34] C.Y. Li, B.L. Gao, X.W. Liu, Q.Y. Fan, X.J. Zhang, G.C. Liu, H.Q. Yang, P.Y. Feng, Y. Wang, P. Song, Quantitative evaluation of the substantially variable morphology and function of the left atrial appendage and its relation with adjacent structures, PLoS ONE 10 (2015), https://doi.org/10.1371/journal.pone.0126818.

[35] J. Park, B. Joung, J.S. Uhm, C. Young Shim, C. Hwang, M. Hyoung Lee, H.N. Pak, High left atrial pressures are associated with advanced electroanatomical remodeling of left atrium and independent predictors for clinical recurrence of

atrial fibrillation after catheter ablation, Heart Rhythm 11 (2014) 953–960, https://doi.org/10.1016/j.hrthm.2014.03.009.
[36] M. Matsuzaki, Y. Toma, R. Kusukawa, Clinical applications of transesophageal echocardiography, Circulation 82 (1990) 709–722, https://doi.org/10.1161/01.CIR.82.3.709.
[37] B.D. Hoit, Y. Shao, M. Gabel, Influence of acutely altered loading conditions on left atrial appendage flow velocities, J. Am. Coll. Cardiol. 24 (1994) 1117–1123, https://doi.org/10.1016/0735-1097(94)90878-8.
[38] N. Fukuda, Transthoracic Doppler echocardiographic measurement of left atrial appendage blood flow velocity: comparison with transoesophageal measurement, Eur. J. Echocardiogr. 4 (2003) 191–195, https://doi.org/10.1016/S1525-2167(02)00166-X.
[39] J.M. Lee, J. Seo, J.S. Uhm, Y.J. Kim, H.J. Lee, J.Y. Kim, J.H. Sung, H.N. Pak, M. H. Lee, B. Joung, Why is left atrial appendage morphology related to strokes? An analysis of the flow velocity and orifice size of the left atrial appendage, J. Cardiovasc. Electrophysiol. 26 (2015) 922–927, https://doi.org/10.1111/jce.12710.
[40] N. Mackman, New insights into the mechanisms of venous thrombosis, J. Clin. Investig. 122 (2012) 2331–2336, https://doi.org/10.1172/JCI60229.
[41] C. Menichini, X.Y. Xu, Mathematical modeling of thrombus formation in idealized models of aortic dissection: initial findings and potential applications, J. Math. Biol. 73 (2016) 1205–1226, https://doi.org/10.1007/s00285-016-0986-4.
[42] A. Sarrami-Foroushani, T. Lassila, S.M. Hejazi, S. Nagaraja, A. Bacon, A.F. Frangi, A computational model for prediction of clot platelet content in flow-diverted intracranial aneurysms, J. Biomech. 91 (2019) 7–13, https://doi.org/10.1016/j.jbiomech.2019.04.045.
[43] B.C. Dickson, Venous thrombosis: on the history of Virchow's Triad, Univ. Tor. Med. J. 81 (2004) 166–171. https://api.semanticscholar.org/CorpusID:19175148.
[44] T. Yamashita, Virchow triad and beyond in atrial fibrillation, Heart Rhythm 13 (2016) 2377–2378, https://doi.org/10.1016/j.hrthm.2016.09.007.
[45] A. Schneider, G. Hommel, M. Blettner, Lineare regressionsanalyse - Teil 14 der serie zur bewertung wissenschaftlicher publikationen, Dtsch. Arztebl. Int. 107 (2010) 776–782, https://doi.org/10.3238/arztebl.2010.0776.
[46] J.F. Ren, D.J. Callans, F.E. Marchlinski, Complicated and impractical classification of LAA morphologies, JACC Cardiovasc. Interv. 9 (2016) 2176–2177, https://doi.org/10.1016/j.jcin.2016.08.023.
[47] K.C. Koskinas, S. Windecker, B. Meier, S. Gloekler, Reply, JACC Cardiovasc. Interv. 9 (2016) 2177–2178, https://doi.org/10.1016/j.jcin.2016.08.030.